AIAA 80-0681R

Buckling of Periodic Lattice Structures

Melvin S. Anderson*
NASA Langley Research Center, Hampton, Va.

Equations are developed for the buckling of a general lattice structure that has repetitive geometry. Equilibrium at a typical node is expressed using finite-element techniques, and the only assumption is that the response is periodic. The stiffness matrix is based on the exact solution of the beam column equation; thus, accurate results are obtained for complex buckling behavior that would require a very large system of equations using conventional techniques. The present method requires the eigenvalues of only a 6×6 determinant. The results are used to study the buckling of isogrid cylinders, three-element truss columns, and polygonal rings. Details of the analysis including expressions for all terms in the governing stability determinant are given.

Nomenclature

a = amplitude of column imperfection
A = cross-sectional area of member
c = cosine of angle denoted by subscript
d_k, e_k, f_k, g_k k = 2, 3; stability functions defined in Eq. (A3)
E = Young's modulus
F_j = force vector at node j, see Eq. (1)
G,H = transformed stiffness matrices defined in Eqs. (A4) and (A5)
GJ = torsional stiffness of member
I_j = moment of inertia of member about x_j axis
k = configuration parameter; $k=1$ for a single laced, $k=2$ for double laced
K = global stiffness matrix
ℓ = length of member
L = length of column
M = mass of column
M_j = moment on end of member about x_j axis
n = circumferential wave number
n_b = number of bays of column
n_s = number of axial or ring members
P = axial load on column
P_{eq} = buckling load of isogrid cylinder with equivalent stiffness properties
P_j = load on end of member in x_j direction
P_0 = self-equilibrating member load due to pretension
P_x = member preload where x is a, c, d, or r
Q = radial load
r = radius of cylinder
R,S = stiffness matrices for member in local coordinates
s = sine of angle denoted by subscript
u_j = displacement at end of member in x_j direction
U_j = displacement vector for node j, see Eq. (1)
x = axial coordinate
x_j = local Cartesian coordinates for member
y_j = $\sqrt{P_x \ell^2 / EI_j}$
α = π / n_s
β = $\pi \ell / \lambda$
γ = angle between cable and x direction
δ = amplitude of deviation of individual member centerline from straight line in x_1 direction
ϵ = $k\beta/2$
θ = angle between diagonal and axial members
λ = longitudinal half wavelength
μ = material density
ρ_k = $\sqrt{EI_k/EA}$, radius of gyration $k=2,3$; if no subscript used, properties are equal in two directions
ϕ = circumferential coordinate
ψ_j = rotation at end of member about x_j axis

Subscripts

a = axial member
c = cable member
d = diagonal member
r = ring member
$1,2,3$ = x_1, x_2, x_3 directions for local member properties, loadings, and displacement
j = node j or a member connecting node 0 to node j

A Greek letter subscript with c or s denotes cosine or sine of that angle.

Superscript

T = transpose of matrix

Introduction

LARGE, low mass lattice structures of the type shown in Fig. 1 are envisioned for future space applications. Lattice booms, platforms, and dishes would be assembled to form structures of unprecedented size. Structural analysis of these components and configurations will require special techniques to cope with the very large number of degrees of freedom. Noor et al.[1] have shown a continuum approach to give good results for overall vibration modes and structural response due to temperature and load inputs.

Detailed response involving bending of individual beams and buckling occurring over relatively few bay lengths, however, is difficult to determine by a continuum approach. The very light loadings and large dimensions expected for space application will lead to very flexible members and require accurate analysis to assure structural integrity. Current approaches are typified by Mikulas[2] where a structural efficiency study was conducted for lightly loaded lattice columns. The basis for the efficiency calculations was Euler buckling of lattice columns and individual elements. For shell-like configurations, the discrete properties were represented by average or "smeared" stiffnesses. Im-

Presented as Paper 80-0681 at the AIAA 21st Structures, Structural Dynamics and Materials Conference, Seattle, Wash., May 12-14, 1980; submitted June 4, 1980; revision received Jan. 11, 1981. This paper is declared a work of the U. S. Government and therefore is in the public domain.

*Principal Scientist, Structural Concepts Branch, Structures and Dynamics Division. Member AIAA.

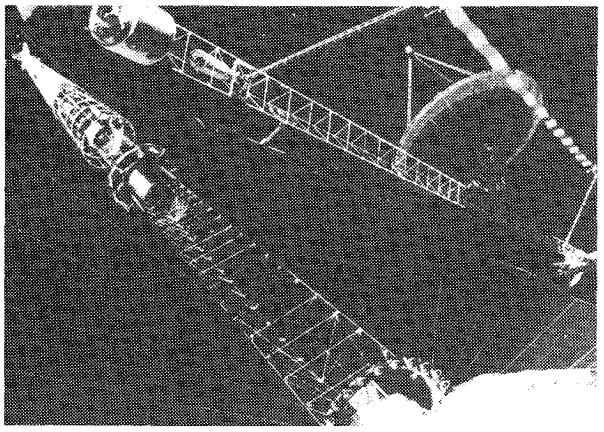

Fig. 1 Lattice structures for space application.

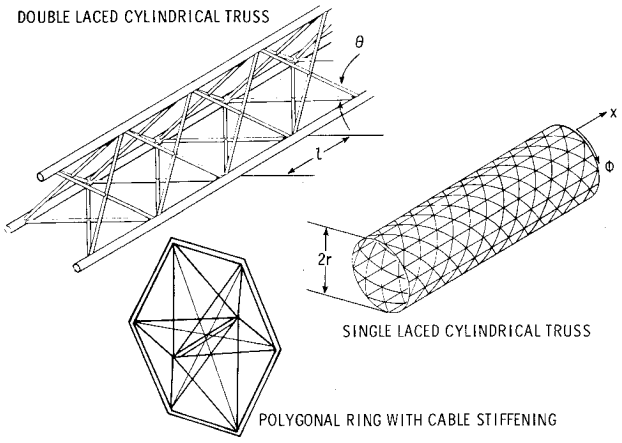

Fig. 2 Lattice configurations analyzed; a) double laced cylindrical truss, b) single laced cylindrical truss, and c) polygonal ring with cable stiffening.

perfections were introduced so that realistic diagonal members would result since there is little theory available for sizing diagonals based on buckling of the perfect structure.

The purpose of the present paper is to develop a simple, yet accurate theory to account for discrete buckling behavior of a class of periodic lattice structures. The theoretical method is an outgrowth of a study by Forman and Hutchinson[3] of buckling of an isogrid cylinder. In the present theory, however, more general expressions are developed, and a straightforward derivation of stiffness and buckling determinants is accomplished in the context of the usual finite-element stiffness matrices. Results for the configurations shown in Fig. 2 are given which illustrate the buckling behavior of these types of structures. In addition, a study of optimum proportions of a special case of the double laced cylinder, a three-element truss column, is given and compared with results of Mikulas.[2]

Analysis

The structure analyzed is assumed to be a periodic lattice such that every internal node is connected to its neighbors in exactly the same geometric pattern. Configurations of this type are shown in Fig. 2. Axial and radial loadings are considered.

The analysis starts with the relation between forces and moments at the end of a single member with the end displacements and rotations. If a member connects node 0 to node j along the x_1 axis, the forces and moments (see Fig. 3a) at node 0 are

$$F_0 = RU_0 + SU_j \tag{1}$$

where

$$F_j^T = (P_1, P_2, P_3, M_1, M_2, M_3)_j$$

$$U_j^T = (u_1, u_2, u_3, \psi_1, \psi_2, \psi_3)_j$$

The two 6×6 matrices, R and S, correspond to the upper half of the usual finite-element stiffness matrix. They are defined in the Appendix along with all other subsequent matrices used. Because the stiffness matrices are based on an exact solution of the beam-column equation under axial load, it is not necessary to introduce intermediate nodes to achieve accurate results. The appearance of the matrices is exactly the same as the conventional linear stiffness matrix except bending terms are modified by the so called stability functions of Livesly and Chandler[4] [Eqs. (A3) in the Appendix] which account for the axial load in the beam. The bending properties in the two principal directions are accounted for in the derivation.

The conventional finite-element transformation matrices are used to write the equilibrium equations at a joint in terms of the displacements of a typical node and the displacements of its neighbors. These equations are as follows for the configurations shown in Fig. 2.

$$\sum_j (G_j U_0 + H_j U_j) = 0 \tag{2}$$

where G_j and H_j are the stiffness matrices resulting from transformation from local member coordinates to global cylindrical coordinates. The summation is over all members that connect at a typical node. The two general configurations, cylinders and rings, are shown in Fig. 3b. The key to the approach is relating the neighbor displacements to the displacements at the node for which equilibrium is written. The assumption of a periodic mode shape in the axial and circumferential directions is found to satisfy the equations exactly. The displacement vector U is then given by

$$U = U_0 e^{i\pi x/\lambda} e^{in\phi} \tag{3}$$

where x is the axial coordinate and ϕ the circumferential coordinate as shown in Fig. 2. The mode shape given by Eq. (3) corresponds to simple support boundary conditions at intervals of λ for the cylindrical configurations. The resulting mode shape has an axial half wavelength λ, and forms n circumferential waves. Equation (3) is used to eliminate unknowns involving adjacent nodal displacements; the equilibrium equation can then be written as

$$KU_0 = 0 \tag{4}$$

where K is the assembled global stiffness matrix. For buckling, the determinant of K is set equal to zero. The

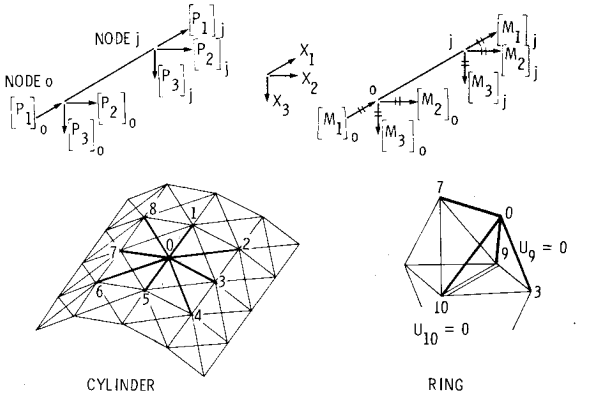

Fig. 3 Member loads and geometry; a) forces and moments on single member and b) typical nodal locations for two general configurations.

components of K are given in the Appendix along with the prebuckling stress state for the various configurations. The use of this finite-element approach facilitates the organization of the analysis so that results for the variety of configurations shown in Fig. 2 having different size members and geometry can be compactly presented. Forman and Hutchinson[3] used a difference operator to relate displacements at two adjacent nodal locations which produces results equivalent to Eq. (3) and results were given for an isogrid configuration (all members equal with helix angles of $\pm 60°$) corresponding to the single laced cylinder of Fig. 2.

Results

The method of Thurston,[5] basically a Newton iteration method, is used to obtain the eigenvalues of the global stiffness matrix [from Eq. (4)]. The buckling behavior of the configuration studied is discussed in subsequent sections.

Isogrid Cylinder

The isogrid cylinder studied by Forman and Hutchinson[3] is analyzed herein to establish the accuracy of the analysis. A typical result for a configuration with 50 longerons having member slenderness ratio $\ell/\rho = 40$ is shown in Fig. 4. The buckling load P is normalized by P_{eq}, the equivalent cylinder buckling load of a circular cylindrical shell having the smeared stiffness properties given by Forman and Hutchinson[3]

$$P_{eq} = \pi(E/\ell)\sqrt{8AI(3+GJ/EI)} \tag{5}$$

The load ratio P/P_{eq} is plotted as a function of buckle length made nondimensional by the cylinder radius. To determine the buckling load for a given length cylinder, it is necessary to examine the loads at $=L/k$ for $k=1, 2, 3, \ldots$, and select the lowest load found. The results are similar to those obtained from accurate shell theory which is capable of predicting results for long wavelength, low n number modes, including the overall Euler buckling load of the cylinder as well as other modes. The classical Euler buckling load is shown by the dashed curve which is slightly higher than the $n=1$ result from the present analysis. This difference occurs because the present theory includes in effect a transverse shear deformation. The discreteness effect for the local buckling mode at $\ell/r < 1$ in Fig. 4 leads to an appreciable reduction (about 20%) from the equivalent cylinder buckling load. The discreteness effect is a function of number of longerons and member slenderness ratio ℓ/ρ, as shown in Fig. 5. The same load parameter (P/P_{eq}) is plotted as a function of ℓ/ρ for three different numbers of stiffeners. The solid curves are for straight helix members and agree with Forman and Hutchinson.[3] If the cylinder has helix members that lie in the curved surface of the circular cylinder, the axial stiffnesses of these members are reduced as indicated by the equation defining the quantity R_{II} in the Appendix. Results for curved helix members are given by the dashed lines in Fig. 5 and show a reduction in buckling load from results for straight helix members.

The isogrid configurations can have many arrangements when wrapped into a cylinder. The one shown in Fig. 5 has axial members and diagonals at $\pm 60°$. The effect on the buckling load of rotating this configuration 90° to produce a $\pm 30°$, 90° arrangement is shown in Fig. 6. The result from Fig. 5 having 50 axial members is also shown in Fig. 6. It is necessary that the parameter n_s be 43 for the $\pm 30°$, 90° configuration in order to have the same radius cylinder for a given member length. For straight members the $\pm 30°$, 90° configuration has a greater buckling capability over most of the ℓ/ρ range. This result is probably due to the fact that for a given axial load, the maximum compressive load in an individual member for the $\pm 30°$, 90° configuration is only ⅔ of the value for the 0°, $\pm 60°$ configuration. The effects of curvature, however, bring the two results close together.

Three-Element Truss Column

Because the analysis in this paper is essentially exact, there is no restriction on number of longerons except that geometric compatibility requires a single laced configuration to have an even number. The double laced configuration can have any number of longerons greater than unity. The simplest configuration is the three-element truss column which is often proposed in structural applications. The buckling charac-

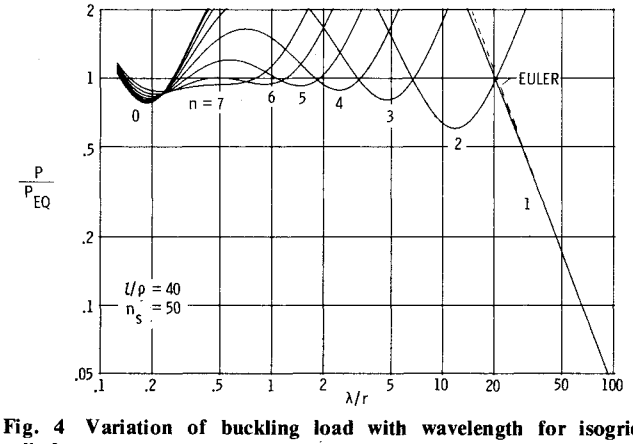

Fig. 4 Variation of buckling load with wavelength for isogrid cylinder.

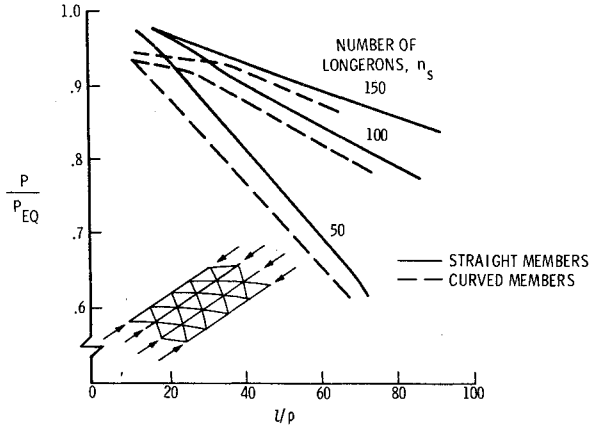

Fig. 5 Effect of number of longerons on buckling of isogrid cylinder.

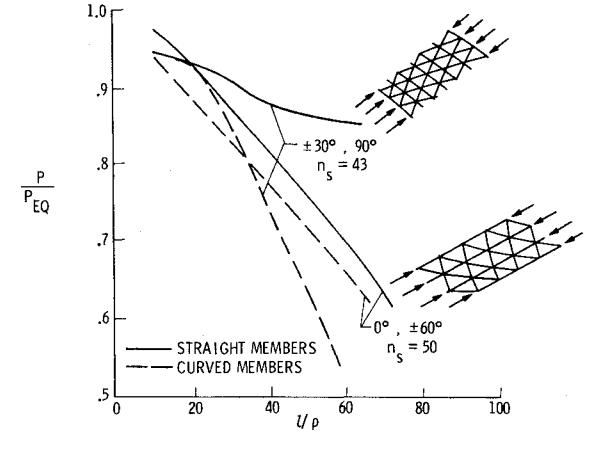

Fig. 6 Effect of member orientation on buckling of isogrid cylinder.

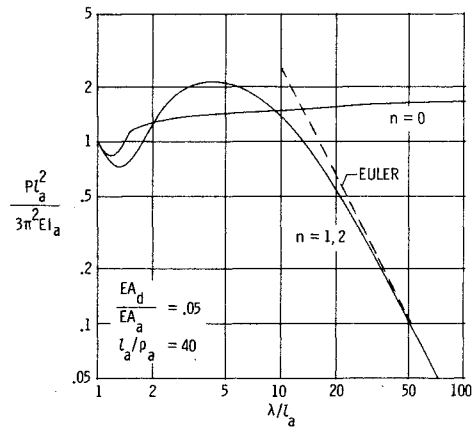

Fig. 7 Variation of buckling load with wavelength of three-element truss column.

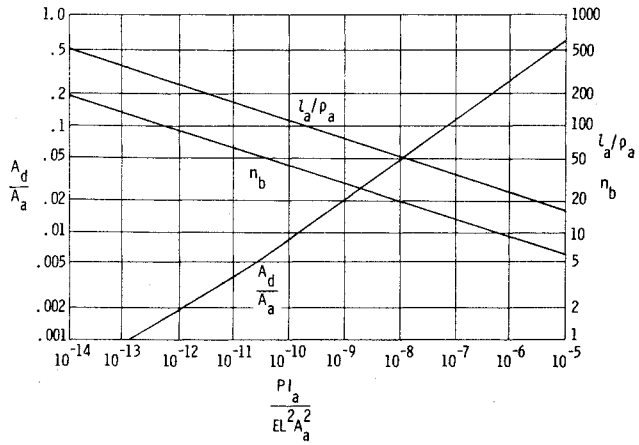

Fig. 8 Optimum proportions of three-element truss column for various axial loadings.

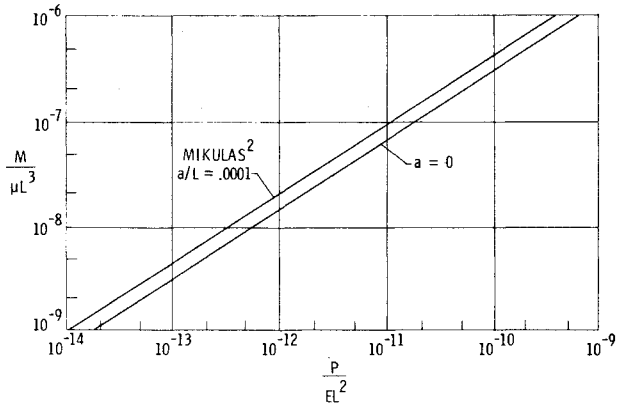

Fig. 9 Structural efficiency of three-element truss column.

teristics of this column will be examined in the next section and used to develop an analysis to determine optimum proportions for minimum mass.

Buckling

The buckling load of the three-element truss column is shown in Fig. 7 for a range of buckle lengths. The load is shown normalized with respect to the load causing Euler buckling of an individual member of length ℓ_a. This load ratio is plotted as a function of buckle length expressed as number of bay lengths, λ/ℓ_a. For a column of a given number of bays, it is necessary to find the wavelength that leads to the minimum buckling load. For this case, columns of 3-17 bays long would buckle in a local mode with a buckle length of approximately $1.5\ell_a$. Beyond 17 bays long the column would buckle in an Euler mode with one half wave. In general the maximum number of circumferential harmonics that need to be considered is equal to the number of longitudinal stiffeners n_s. For the case of $n_s = 3$, however, identical results are produced for $n = 1$ and $n = 2$, therefore only two curves are shown in Fig. 7. Again the $n = 1$ result in Fig. 7 corresponds to the overall column buckling load with an effective shear correction factor for shorter wavelengths.

Optimization

A commonly used approach for optimization calculations is to equate the Euler buckling load of individual members to the overall column buckling load. As can be seen from Fig. 7, two things can cause the resulting design to be nonconservative. First, the overall Euler load may not be achieved because of transverse shear deformation (25% reduction at $\lambda/\ell_a = 20$). Second, the size of the diagonal members supporting the longitudinal members may be insufficient to form a node and local buckling would occur involving nodal deflections at loads less than the Euler load of the bay. For the example in Fig. 7, this reduction is almost 30% occurring at $\lambda/\ell_a = 1.5$. Introducing an imperfection to produce a load in the diagonal was used by Miklulas[2] to size the diagonal members, and it was assumed that the resulting member sizes would prevent the lower local modes from occurring.

With the use of the present analysis, proportions can be found which force the local minima shown in Fig. 7 to rise above the individual member Euler load. The longest column length that will support the Euler load for buckling of one bay then can be determined easily from a plot such as Fig. 7. Numerical calculations have shown this procedure produces nearly optimum design. The resulting proportions for solid section columns are shown in Fig. 8 as a function of nondimensional structural index $(P/EL^2)(I_a/A_a^2)$. The use of the shape factor, I_a/A_a^2, allows results for a wide range of section characteristics, from solid to tubular, to be presented as single curves. The area of diagonals relative to the area of longeron, A_d/A_a, ℓ_a/ρ_a of an individual longeron, and number of bays n_b is given. A structural efficiency diagram using proportions from Fig. 8 was determined and is shown in Fig. 9. The column mass M of material of density μ is shown in the nondimensional mass index $M/\mu L^3$ for the solid rod truss column. Results from Mikulas[2] for the smallest imperfections considered have greater mass than that determined from the present analysis due to the consideration of an imperfection and an allowance of 15% for the mass of joints. The present analysis, however, has the effect of transverse shear deformations which would tend to make the mass higher than found by Mikulas.[2]

Polygonal Ring

Some concepts for large lightweight surfaces in space involve a stretched membrane supported at the vertices of a polygonal ring. The inward radial load produces compression in the ring members that can cause buckling. Such a structure can be treated by retaining only those terms involving ring members. It is necessary to preclude $n = 0$ and 1 responses that represent rigid body modes for which the determinant of K is zero at zero load. A study was made of the buckling of such a ring with and without cable stiffening.

Unstiffened Ring

The results shown in Fig. 10 for buckling of an unstiffened ring are in terms of a buckling parameter $Qr^3/\ell_r EI_r$ equivalent to the classical ring buckling parameter. Results are shown as a function of number of sides of the ring. Two eigenvalues were found, the lowest corresponds to out-of-plane buckling and the second corresponds to an inplane mode. Results from the direct application of Eq. (4) correspond to constant direction or dead loading. In certain

structures the radial load may be due to forces exerted by membrane action from a thin reflector or antenna surface. In this case it is more realistic to consider the load as always directed toward the center. An external load of magnitude Qu_1/r in the axial direction and Qu_2/r in the circumferential direction was added to the equations in the Appendix to give this result. All four curves are shown in Fig. 10 and for large number of sides agree with circular ring theory results.[6-8] For small number of sides there are some variations in the buckling parameters. For three sides there is a significant increase in the out-of-plane buckling load.

Cable Stiffened Ring

The cable stiffened ring has a rigid mast perpendicular to the plane of the ring that is located symmetrically (see Fig. 2). (A flexible mast would increase the complexity of the problem but the assumption of a rigid mast is believed to be reasonable for many practical problems.) Members characterized as cables connect from the end of the mast to each vertex of the polygon. The stiffness of these members used in the numerical results was small compared to that of the ring so that their compressive load capability is essentially zero. Thus, the cables must be pretensioned in order to be effective.

In Fig. 11 the buckling load Q in terms of the same ring buckling parameter used in Fig. 10 is plotted against a nondimensional pretension parameter. Also plotted is the internal load in the ring P_r. The parameters used in the figure tend to make the results independent of the number of sides for $n_s > 20$. The results were obtained for $n_s = 50$ and $EA_c/EA_r = 0.001$ with a few calculations made at other values of n_s. The portion of the curve with positive slope represents

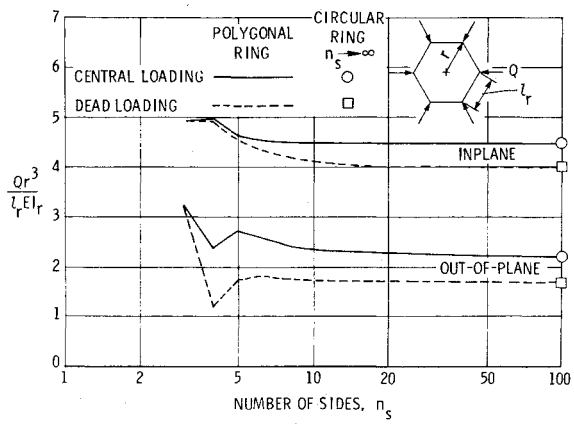

Fig. 10 Buckling of polygonal ring.

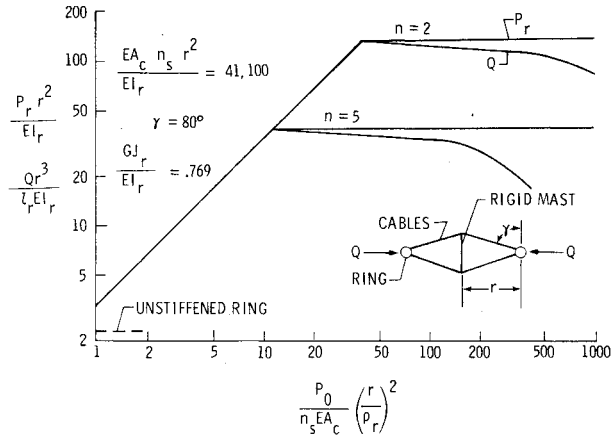

Fig. 11 Effect of pretension on buckling of cable stiffened ring (central loading).

the load required to make the cables go slack. A point is reached where ring buckling occurs and further increases of pretension actually cause a slight decrease in the buckling load Q. However, the internal load P_r is essentially constant. For an unstiffened ring, the minimum buckling load occurs for $n = 2$. For the case shown, the minimum buckling load at higher values of P_0 is for $n = 5$ and is considerably smaller than the $n = 2$ load. For a given angle γ the level of the maximum buckling load is a function of the parameter $n_s r^2 EA_c/EI_r$ as long as there are sufficient number of sides to preclude buckling between cable attachments. The results shown are for a central loading and show that a substantial increase in ring buckling capability compared to the unstiffened ring is possible for a rather short mast. Practical consideration of such factors as temperature changes and imperfections require that the pretension be well beyond that required to achieve the maximum load Q. The slow drop off of Q with pretension allow such high pretension loads with little loss in buckling capability.

Concluding Remarks

A simple but accurate buckling analysis is developed for periodic lattice structures. For lattices with each node having identical geometry with respect to its neighbors, a periodic trigonometric mode shape satisfies the governing equations. The buckling load is determined from the eigenvalues of a 6×6 matrix. Results are given for an isogrid cylinder, a three-element truss column, and a polygonal ring. The effect of having discrete members rather than a homogeneous structure can be substantial for the isogrid cylinder and the three-element truss column compared to results from equivalent shell or beam theory, and this effect increases as the lattice member slenderness ratio increases. Member orientation and member curvature was also a significant effect in buckling of the isogrid cylinder. The analysis is applied successfully to finding optimum proportions of a solid-rod three-element truss column. The mass characteristics found were in reasonable agreement with that found in a previous study based on somewhat different assumptions and a simpler analysis. A study of a polygonal ring yields results which agreed with circular ring theory as number of sides exceeds 20. A significant increase in ring buckling load was shown to be possible by the addition of pretensioned cable stiffening.

Appendix

Development of Global Stiffness Matrix

The analysis is applicable to repetitive structures of the type shown in Fig. 2 that have only one typical geometry for connecting members of adjacent nodes as shown in Fig. 3b. The assumption of a rigid mast for the cable stiffened ring removes the nodes at the end of the mast from the analysis so the criterion of having only one typical node is satisfied. The assumption of a periodic buckle pattern [Eq. (2)] makes possible simple but accurate treatment of complex configurations. Details of the finite-element type development of the matrix equation follow.

Matrix Equations Used in the Analysis

A typical node (node 0) is shown in Fig. 3b with various members connecting to adjacent nodes. It is assumed that elastic properties and loads are identical for certain groups of members as follows: axial members connect to nodes 1, 5 denoted with subscript a; diagonal members connect to nodes 2, 4, 6, 8 denoted with subscript d; ring members connect to nodes 3, 7, denoted with subscript r; and cable members connect to nodes 9, 10 denoted with subscript c. The analysis starts with the fundamental stiffness matrices, as used in Eq.

(1), for a member aligned with the x_1 axis

$$R=\begin{bmatrix} R_{11} & 0 & 0 & 0 & 0 & 0 \\ & R_{22} & 0 & 0 & 0 & R_{26} \\ & & R_{33} & 0 & R_{35} & 0 \\ & & & R_{44} & 0 & 0 \\ & SYM & & & R_{55} & 0 \\ & & & & & R_6 \end{bmatrix} \quad \text{(A1)}$$

$$S=\begin{bmatrix} S_{11} & 0 & 0 & 0 & 0 & 0 \\ 0 & S_{22} & 0 & 0 & 0 & S_{26} \\ 0 & 0 & S_{33} & 0 & S_{35} & 0 \\ 0 & 0 & 0 & S_{44} & 0 & 0 \\ 0 & 0 & -S_{35} & 0 & S_{55} & 0 \\ 0 & -S_{26} & 0 & 0 & 0 & S_{66} \end{bmatrix} \quad \text{(A2)}$$

where

$$R_{11}=\frac{EA/\ell}{1+8/15\left[\frac{(\delta_2/\rho_3)^2}{(1-(y_3/\pi)^2)^3}+\frac{(\delta_3/\rho_2)^2}{(1-(y_2/\pi)^2)^3}\right]}$$

$$R_{22}=12g_3EI_3/\ell^3 \qquad R_{26}=6f_3EI_3/\ell^2$$

$$R_{33}=12g_2EI_2/\ell^3 \qquad R_{35}=-6f_2EI_2/\ell^2$$

$$R_{44}=GJ/\ell \qquad R_{55}=4d_2EI_2/\ell \qquad R_{66}=4d_3EI_3/\ell$$

$$S_{11}=-R_{11} \qquad S_{22}=-R_{22} \qquad S_{26}=R_{26}$$

$$S_{33}=-R_{33} \qquad S_{35}=R_{35} \qquad S_{44}=-R_{44}$$

$$S_{55}=2e_2EI_2/\ell \qquad S_{66}=2e_3EI_3/\ell \quad \text{(A3)}$$

$$d_j=y_j(\sin y_j-y_j\cos y_j)/4\Delta_j \qquad e_j=y_j(y_j-\sin y_j)/2\Delta_j$$

$$f_j=y_j^2(1-\cos y_j)/6\Delta_j \qquad g_j=y_j^3\sin y_j/12\Delta_j$$

$$\Delta_j=2-2\cos y_j-y_j\sin y_j \qquad y_j=\sqrt{(P_x\ell^2/EI_j)}$$

$$\lim_{y_j\to 0}\begin{matrix} d_j \\ e_j \\ f_j \\ g_j \end{matrix}=1$$

P_x is prestress load in member where x may be a, c, d, or r

The expression for the axial stiffness R_{11} has been adjusted to account for an imperfection based on the beam column solution for a simply supported beam. The error in this approximation when the ends are not simply supported and the effect on buckling calculations are not known at this time.

The matrices in Eq. (2) are defined by transformation of coordinates as follows:

$$G=T^TRT \quad \text{(A4)}$$

$$H=T^TST' \quad \text{(A5)}$$

where

$$T=\begin{bmatrix} W & 0 \\ 0 & W \end{bmatrix} \quad \text{(A6)}$$

$$W=\begin{bmatrix} c & sc & ss \\ -s & cc & cs \\ 0 & -s & c \end{bmatrix} \quad \text{(A7)}$$

$$T'(\beta,\epsilon)=T(\beta,-\epsilon) \quad \text{(A8)}$$

The values of β and ϵ vary for each member as shown in Table 1.

The final global stiffness matrix K, which is symmetric, is defined as follows:

$$K_{11}=[2(R_{11}+S_{11}c_\beta)]_a+pQ/r+[4(R_{22}+S_{22}c_\epsilon c_\eta)s_\theta^2$$
$$+4(R_{11}+S_{11}c_\epsilon c_\eta)c_\theta^2]_d+[2(R_{22}+S_{22}c_\tau)]_r$$
$$+[2(R_{11}c_\gamma^2+R_{22}s_\gamma^2)]_c$$

$$K_{12}=[4(S_{22}-S_{11})c_\theta s_\theta c_\alpha s_\epsilon c_\eta]_d$$

$$K_{13}=[4(S_{22}-S_{11})c_\theta s_\theta s_\alpha s_\epsilon c_\eta]_d$$

$$K_{14}=0$$

$$K_{15}=[4(R_{26}-S_{26}c_\epsilon c_\eta)s_\theta s_\alpha]_d$$
$$+[2(R_{26}-S_{26}c_\tau)s_\alpha]_r+[2R_{26}s_\gamma]_c$$

$$K_{16}=[-4S_{26}s_\theta c_\alpha c_\epsilon s_\eta]_d+[-2S_{26}c_\alpha s_\tau]_r$$

$$K_{22}=[2(R_{22}+S_{22}c_\beta)]_a+[4(R_{33}-S_{33}c_\epsilon c_\eta)s_\alpha^2$$
$$+4(R_{11}+S_{11}c_\epsilon c_\eta)s_\theta^2c_\alpha^2+4(R_{22}+S_{22}c_\epsilon c_\eta)c_\theta^2c_\alpha^2]_d$$
$$+[2(R_{11}+S_{11}c_\tau)c_\alpha^2+2(R_{33}-S_{33}c_\tau)s_\alpha^2]_r$$
$$+[2R_{33}]_c+pQ/r$$

$$K_{23}=[-4(S_{11}s_\theta^2+S_{22}c_\theta^2+S_{33})c_\alpha s_\alpha c_\epsilon s_\eta]_d$$
$$+[-2(S_{11}+S_{33})c_\alpha s_\alpha s_\tau]_r$$

$$K_{24}=[4(R_{35}+S_{35}c_\epsilon c_\eta)s_\theta s_\alpha]_d$$
$$+[2(R_{35}+S_{35}c_\tau)s_\alpha]_r+[2R_{35}s_\alpha]_c$$

$$K_{25}=[4(S_{35}-S_{26})c_\theta c_\alpha s_\alpha s_\epsilon s_\eta]_d$$

$$K_{26}=[2S_{26}s_\beta]_a+[4(S_{35}s_\alpha^2+S_{26}c_\alpha^2)c_\theta s_\epsilon c_\eta]_d$$

$$K_{33}=[2(R_{33}+S_{33}c_\beta)]_a+[4(R_{11}-S_{11}c_\epsilon c_\eta)s_\theta^2s_\alpha^2$$
$$+4(R_{22}-S_{22}c_\epsilon c_\eta)c_\theta^2s_\alpha^2+4(R_{33}+S_{33}c_\epsilon c_\eta)c_\alpha^2]_d$$
$$+[2(R_{11}-S_{11}c_\tau)s_\alpha^2+2(R_{33}+S_{33}c_\tau)c_\alpha^2]_r$$
$$+[2(R_{11}s_\gamma^2+R_{22}c_\gamma^2)]_c$$

Table 1 β and ϵ values for each member

j	1	2	3	4	5	6	7	8	9	10
β	0	θ	$\pi/2$	$\pi-\theta$	π	$\pi+\theta$	$3\pi/2$	$-\theta$	γ	$\pi-\gamma$
ϵ	0	α/q	α	α/q	0	$-\alpha/q$	$-\alpha$	$-\alpha/q$	$\pi/2$	$\pi/2$

$$K_{34} = [4S_{35}s_\theta c_\alpha c_\epsilon s_\eta]_d + [2S_{35}c_\alpha s_\tau]_r$$

$$K_{35} = [-2S_{35}s_\beta]_a + [-4(S_{35}c_\alpha^2 + S_{26}s_\alpha^2)c_\theta s_\epsilon c_\eta]_d$$

$$K_{36} = [4(S_{35} - S_{26})c_\theta c_\alpha s_\alpha s_\epsilon s_\eta]_d$$

$$K_{44} = [2(R_{44} + S_{44}c_\beta)]_a + [4(R_{55} + S_{55}c_\epsilon c_\eta)s_\theta^2 + 4(R_{44} + S_{44}c_\epsilon c_\eta)c_\theta^2]_d + [2(R_{55} + S_{55}c_\tau)]_r + [2(R_{44}c_\gamma^2 + R_{55}s_\gamma^2)]_c$$

$$K_{45} = [4(R_{44} + S_{55})c_\theta s_\theta c_\alpha s_\epsilon s_\eta)]_d$$

$$K_{46} = [4(R_{44} + S_{55})c_\theta s_\theta s_\alpha s_\epsilon c_\eta)]_d$$

$$K_{55} = [2(R_{55} + S_{55}c_\beta)]_a + [4(R_{66}s_\alpha^2 + R_{55}c_\theta^2 c_\alpha^2) + 4(R_{44} + S_{44}c_\epsilon c_\eta)s_\theta^2 c_\alpha^2 - 4(S_{66}s_\alpha^2 - S_{55}c_\theta^2 c_\alpha^2)c_\epsilon c_\eta)]_d + [2(R_{66}s_\alpha^2 - S_{66}s_\alpha^2 c_\tau) + 2(R_{44} + S_{44}c_\tau)c_\alpha^2]_r + [2R_{66}]_c$$

$$K_{56} = [-4(S_{66} + S_{55}c_\theta^2 + S_{44}s_\theta^2)c_\alpha s_\alpha c_\epsilon s_\eta]_d - [2(S_{66} + S_{44})c_\alpha s_\alpha s_\tau]_r$$

$$K_{66} = [2(R_{66} + S_{66}c_\beta)]_a + [4(R_{66}c_\alpha^2 + R_{55}c_\theta^2 s_\alpha^2) + 4(S_{66}c_\alpha^2 - S_{55}c_\theta^2 s_\alpha^2)c_\epsilon c_\eta + 4(R_{44} - S_{44}c_\epsilon c_\eta)s_\theta^2 s_\alpha^2]_d + [2(R_{66}c_\alpha^2 + S_{66}c_\alpha^2 c_\eta) + 2(R_{44} - S_{44}c_\tau)s_\alpha^2]_r + [2(R_{44}s_\gamma^2 + R_{55}c_\gamma^2)]_c \quad \text{(A9)}$$

where

$$\alpha = \pi/n_s, \qquad \beta = \pi\ell/\lambda, \qquad \epsilon = k\pi\ell/2\lambda$$

$k = 1$ single laced, $k = 2$ double laced $\tau = 2n\alpha$

$\eta = 2n\alpha/q$, $p = 0$ dead load $p = 1$ central load

$q = 2$ for configurations with single laced diagonal members having ring members

$q = 1$ otherwise

Prebuckling Stress State

Cylindrical Configurations

The prestress state determined for the cylindrical lattices loaded by an axial load P is

$$P_a = PZ/n_s + P_0$$

$$P_d = P(1-Z)/(2n_s\cos\theta) - P_0/(2\cos\theta)$$

$$P_r = \frac{[(-P(1-Z)\tan\theta)/n_s + P_0\tan\theta]\sin(\alpha/q)}{\sin\alpha}$$

where

$$Z = 1\Big/\left[1 + \frac{2\ell_a^3 EA_r EA_d}{EA_a(EA_r\ell_d^3 + 2EA_d\ell_r^3)}\right]$$

The terms involving P_0 are only applicable when axial, helical, and ring members are all present.

Ring Configurations

The prestress state for ring configurations loaded by a radial force Q at each vertex is

$$P_r = Q/2(\sin\alpha + EA_c/EA_r\sin^3\gamma) + P_0$$

$$P_c = \frac{(QEA_c/EA_r)}{2(\sin\alpha + EA_c/EA_r\sin^3\gamma)} - P_0\sin\alpha/\sin\gamma$$

The terms involving P_0 are only applicable when both ring and cable members are present.

References

[1] Noor, A. K., Anderson, M. S., and Greene, W. H., "Continuum Models for Beam- and Plate-like Lattice Structures," *AIAA Journal,* Vol. 16, Dec. 1978, pp. 1219-1228.

[2] Mikulas, M. M. Jr., "Structural Efficiency of Long Lightly Loaded Truss and Isogrid Columns for Space Application," NASA TM 78687, July 1978.

[3] Forman, S. E. and Hutchinson, J. W., "Buckling of Reticulated Shell Structures," *International Journal of Solids and Structures,* Vol. 6, July 1970, pp. 909-932.

[4] Livesly, R. K. and Chandler, D. B., *Stability Functions for Structural Frameworks,* Manchester Univ. Press, Manchester, 1956.

[5] Thurston, G. A., "Roots of Lambda Matrices," *Journal of Applied Mechanics,* Vol. 45, Dec. 1978, pp. 859-863.

[6] Ratzersdorfer, J., "The Buckling of a Thin Circular Arch," *Engineering,* Vol. 150, Oct. 11, 1940, pp. 284-285.

[7] Boresi, A. P., "A Refinement of the Theory of Buckling of Rings Under Uniform Pressure," *Journal of Applied Mechanics,* Vol. 22, March 1955, pp. 95-102.

[8] Timoshenko, S. and Gere, J., *Theory of Elastic Stability,* 2nd ed., McGraw-Hill Book Co., Inc., 1961, pp. 313-318.